npj | Materials Degradation

www.nature.com/npjmatdeg

ARTICLE OPEN

Check for updates

Corrosion inhibition of locally de-passivated surfaces by DFT study of 2-mercaptobenzothiazole on copper

Fatah Chiter[1]✉, Dominique Costa[1], Vincent Maurice[1] and Philippe Marcus[1]✉

Investigating the interaction of organic inhibitors with metal and alloy surfaces is crucial for an atomic-scale understanding of their protection efficiency, particularly on the initiation of localized corrosion by pitting. Quantum chemical DFT calculations were performed to optimize the constructed model of a depassivated copper surface and to study the adsorption of 2-mercaptobenzothiazole (MBT), on different zones exposed by local depassivation. Reactive sites exist at the metal surface, at the oxide surface, as well as on the oxide edges and oxide walls. The surface-reactive sites are the unsaturated and saturated copper atoms and singly and doubly unsaturated oxygen atoms of the oxide, and the copper atoms of the metal. The sulfur (S_{exo} and S_{endo}) and nitrogen (N or NH) atoms are the reactive sites in the molecules. MBT can covalently bond to the oxide surface as well as to the oxide edges, oxide walls, and metal surface exposed by depassivation. For the thione species, local adsorption strength decreases as oxide edges > oxide surface > metal surface > oxide walls, suggesting that MBT heals the low coordinated sites. For the thiolate species, adsorption strength is similar on the different area, except the oxide walls. The results show the ability of the inhibitor to interact on different zones of a locally depassivated surface and to form a strongly adsorbed organic film, which can block the initiation of localized corrosion by enhancing the interfacial barrier properties, including in the local surface areas incompletely passivated or locally damaged by depassivation.

npj Materials Degradation (2021)5:52; https://doi.org/10.1038/s41529-021-00198-x

INTRODUCTION

The use of organic inhibitors is one of the major ways to mitigate the corrosion of metals and alloys[1–3]. The inhibitor adsorbs on the metal (or alloy) surface, forming a protective film. This organic film acts as a physical and/or chemical barrier against diffusion of aggressive species from the environment to the metal or alloy substrate and can prevent its dissolution. Numerous experimental[3–5] and theoretical works[6–9] have been carried out to show the efficiency of various organic compounds as corrosion inhibitors to protect the metal and also for a better understanding of the inhibitor-surface interaction, as well as the inhibition mechanisms.

Among the organic corrosion inhibitors, 2-mercaptobenzothiazole (MBT) has been shown to improve the corrosion resistance of metal and alloys, using various experimental techniques and conditions[10–32]. The mechanisms of MBT/surface interaction are complex because (i) the MBT molecule presents different active sites (S, N, and NH) that may interact differently with the surface, (ii) MBT may be present in various forms (thiol, thione, and anionic), (iii) the metal may exhibit different surface states (metallic, oxidized, i.e., passivated by a surface oxide, or partially oxidized states). All these factors play a key role on the reactivity and efficiency of the inhibitors.

On copper, numerous studies in different experimental conditions[33–37] showed that the adsorption of MBT molecule on copper surface improves the protection of the metal against corrosion and acts as mixed-type (i.e., anodic and cathodic) inhibitor[35,36,38–40]. The characteristics of the organic film depend on the stability domain and the thickness of the passivating surface oxide[34,41]. In the Cu_2O-stability domain (pH > 4), the organic films exhibit monolayer thickness, whereas in the Cu_2O-instability domain (pH < 3), they exhibit multilayer thickness[34]. The presence of the copper ions in the solutions allows to increase the thickness of the protective film to any desired value[34]. MBT organic layers formed on the oxide free Cu surface prevent oxide formation in solution[42] and at ultralow pressure in gas phase[43,44]. Some works suggest that the interaction mechanism consists in direct surface reaction between MBT and copper[33] or from precipitation of Cu–MBT complex[34,35].

Experimentally, the adsorption of MBT on Cu surface was concluded to involve both N and S atoms[38,41]. However, Woods et al.[27] reported that the interaction of MBT with copper, silver, and gold surfaces involves only the bonding between the exocyclic S and metal atoms. In controlled experimental conditions at the atomic scale, the bonding via the two S atoms to Cu atoms was also concluded for adsorption in the monolayer from the gas phase on oxide-free Cu(111) surfaces[43,44]. In contrast, Shahrabi et al.[39] supposed that the bonding between inhibitor molecules and copper surface is only via electrostatic interactions.

In order to understand the adsorbate–metal-interaction details, quantum chemical DFT modeling can be performed in correlation with the experimental conditions. The model of a Cu(hkl) metal slab is used to mimic the copper surface chemical state in acidic solutions (pH < 5)[45,46], in alkaline solutions in the underpotential range of oxide formation[47–49], and at ultra low pressure in gas phase[43,44]. For example, MBT was found to better protect the Cu (220) surface than Cu(200) and Cu(111) surfaces in the metallic state at low Cl concentration, due to the higher chemical activity of (220) face[50]. The results were correlated to density functional theory (DFT) calculations and showed that MBT is adsorbed via chemical bonding on Cu(220) surface, involving the two sulfur atoms, while it was physically bonded via electrostatic interactions on Cu(200) and Cu(111) surfaces[50]. Vernack et al.[51] investigated by DFT the adsorption of MBT under different species (thiol, thione, and thiolate) on the Cu(111) metallic surface. They concluded that the molecules can be strongly adsorbed in a perpendicular orientation at high coverage, bonded via the terminal S atom. The

[1]PSL University, CNRS - Chimie ParisTech, Institut de Recherche de Chimie Paris/Physical Chemistry of Surfaces Group, 11 rue Pierre et Marie Curie, 75005 Paris, France. ✉email: fatah.chiter@chimieparistech.psl.eu; philippe.marcus@chimieparistech.psl.eu

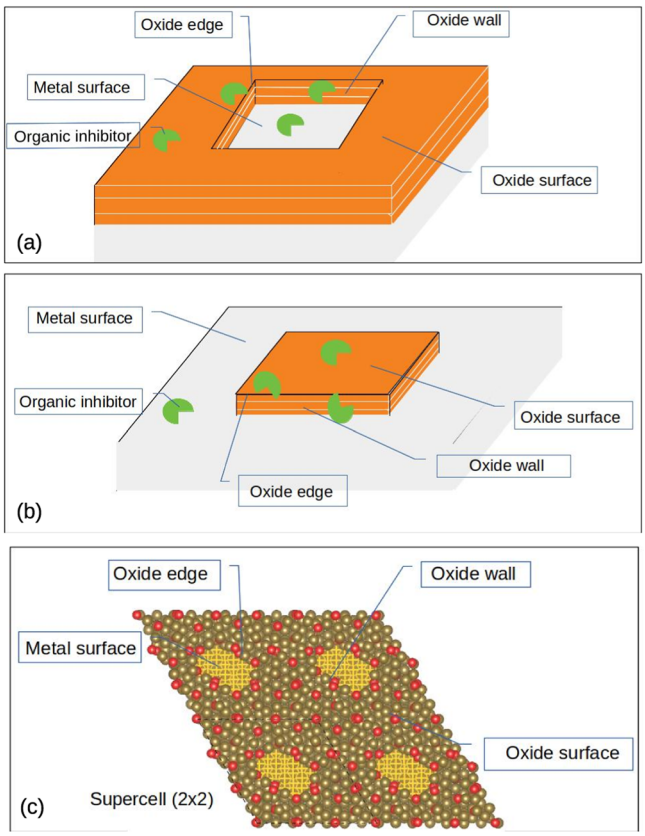

Fig. 1 Model of the partially oxide-covered copper surface. **a** Local depassivation. **b** Incomplete passivation. **c** Locally depassivated surface contains oxide and metal parts, oxide edges, and oxide walls, on which the organic inhibitor may adsorb differently.

thiolate species forms a more stable film on Cu(111) surface, adopting a (3×3) superstructure.

In contrast, computational models composed of non supported $Cu_2O(111)$[52–55] and supported $Cu(111)||Cu_2O(111)$[56] oxide surfaces are used to study adsorption on oxidized copper surfaces. The models reproduce the electrochemical state of oxidized copper surface[57–61]. Recently, in order to gain atomic-scale insight into the corrosion inhibition properties of MBT and MBI molecules on the most realistic interfacial model, we performed quantum chemical DFT calculations of the interaction of molecules on the passivated copper surfaces (Cu(111) surface covered by an ultrathin $Cu_2O(111)$ oxide)[62,63]. For both thione (MBTH) and thiolate (MBT°) forms of MBT inhibitor, the formation of a full monolayer (ML) was demonstrated and the thiolate form had the strongest adsorption bonding. MBTH was found to bind covalently on the oxidized copper surface via the exocyclic S atom and to form an H-bond via the NH group, whereas MBT° was found to form two covalent bonds via the exocyclic S and N atoms. We also showed that both forms of MBT can form organic layers by substitution of water and OH group at the hydrated and hydroxylated Cu_2O surface, respectively[62].

The adsorption of MBT and the formation of organic films on metallic, passivated and oxidized copper surfaces is well established. Whereas information at the atomic scale on well-defined metal-surface terminations is precious, they are not sufficient to understand the adsorption behavior of the inhibitor molecule on an incompletely passivated metal surface, i.e., partially covered by a surface oxide, and especially at the metal/oxide borders. An incompletely passivated surface may exist if oxide growth does not saturate the metal substrate or if the metal substrate has been locally exposed as a result of local breakdown of passivity caused by aggressive agents or mechanical loading. In other words, whether an inhibitor molecule can efficiently heal a depassivated zone and protect it from pit nucleation remains, to the best of our knowledge, a key, unanswered question.

In the present work, we addressed this question with MBT on partially depassivated copper as a first step toward the atomic-scale understanding of the prevention of the initiation of localized corrosion by pitting. Quantum chemical DFT calculations were applied to the adsorption of MBT in thione or thiolate forms on a model of the copper surface incompletely covered by a surface oxide film. A Cu(111) surface covered by an ultrathin Cu_2O oxide film ($Cu(111)||Cu_2O(111)$) derived from experimental data was used for the modeling of the incompletely passivated copper surface. The MBT species were adsorbed to form a monolayer at high coverage. We investigated structural, energetic, and electronic properties of the adsorption configurations.

RESULTS

Partially oxide-covered copper surface ($Cu(111)||Cu_2O(111)$-hole model)

Our aim in this work is to study the adsorption of the organic inhibitor on the incompletely passivated or locally depassivated copper surface, locally exposing copper metal, and thus susceptible to the initiation of pitting in aggressive environments. Such a situation can occur if the growth of the passive film does not saturate the surface (incomplete passivation), or after local breakdown at the most fragile sites of the passive film (local depassivation). It leads to the presence of different local areas on the partially oxide-covered surface, with different reactivities. The surface exposes metal and oxide, as well as oxide edges and oxide walls in the interfacial areas between the metal and oxide parts, like illustrated in Fig. 1. Therefore, the adsorption properties of the molecules on these different parts of the partially oxide-covered copper will be dissimilar, and we can expect the corrosion-inhibition mechanism to differ depending on the local bonding and adsorption capability of the molecules. Molecules that would fully heal the defect would be best inhibitors.

Modeling partially oxide-covered metal surfaces remains a great challenge for periodic calculations based on DFT, due to the large size of the systems (in the order of nanometer), which requires considerable resources and calculation times. We opted for the formation of a hole in the surface oxide initially covering the metal surface as shown in Fig. 1a–c. This system is well adapted to describe incomplete passivation of local depassivation and allows for the investigation of the adsorption of the organic molecules on the different parts of the partially oxide-covered surface, i.e., oxide surface, metal surface, oxide edges, and oxide walls.

Based on quantum chemical DFT calculations, we constructed and optimized an oxide-covered copper surface model[56], which was derived from experimental measurements[48,60,61,64]. We detailed the structural, electronic properties, and the reactivity of the surface toward water molecules and OH groups[56]. The model was also used to study by DFT the adsorption of MBT[62] and MBI[63] on the oxidized copper surface. Because the adsorption of MBT on the oxidized copper surfaces with an intact oxide film showed that the adsorption energies were similar with two and four oxide layers, we focused in the present work only on the two-layer thick oxide. The choice of a 2-layer thick oxide was done on the one hand to avoid too heavy computational calculations, on the other hand, to model a preoxidized surface with a noncontinuous ultrathin oxide layer. Such surfaces need to be further protected against corrosion by organic inhibitors.

Starting from this $Cu(111)||Cu_2O(111)$ model, the approach used in the present work for the construction of the hole in the oxide consists in removing certain copper and oxygen atoms from the surface and interface oxide layers as described hereafter. To

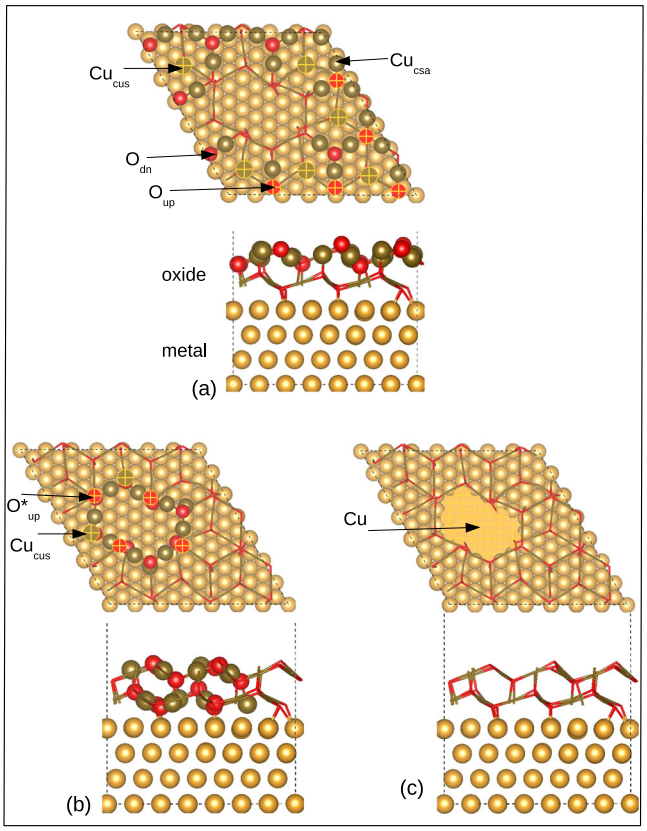

Fig. 2 Reactive sites on the partially oxide-covered copper surface. a Oxide surface, **b** oxide edges and oxide-wall surface, and **c** metal surface.

generate the hole in the oxide, we removed eight atoms of copper and two atoms of oxygen, which correspond to four copper and one oxygen atom in each oxide layer (surface and undersurface oxide layers). It allows us to generate oxide holes with stable walls, meaning that the facets are stable. The hole in the oxide has a near-hexagonal shape and represents 11.11% (0.305 nm^2) of the oxide-surface area. Now, the surface exposes the Cu(111) metal, the $Cu_2O(111)$ oxide and the oxide edges and oxide walls at the interface between the two (Fig. 1c). This model is simple enough, stable, practical, and reflects well the different parts of partially oxide-covered copper surface. This approach can be extended to study the oxide-island formation on a metal surface.

The bare surface exhibits several distinct copper and oxygen atomic sites, as shown in Fig. 2. The oxide part is identical to the perfect $Cu_2O(111)$ surface. It exhibits copper- (Cu_{csa}) and oxygen- (O_{dn}) saturated atoms, and copper- (Cu_{cus}) and oxygen- (O_{up}) unsaturated atoms. The walls and the edges of the hole in the oxide also expose Cu_{csa} and Cu_{cus} sites and O_{dn} and O_{up} sites. In addition, they exhibit oxygen sites labeled O^*_{up}, which are bonded to only two copper atoms. In contrast, the O_{dn} and O_{up} atoms form four and three bonds with copper atoms, respectively. Finally, the metal part contains only the metal Cu atoms with top, bridge, and hollow sites.

Adsorption of MBT on the partially oxide-covered copper surfaces

The MBT molecule was modeled in thione (MBTH) and radical thiolate (MBT°) forms. The thiol conformer is less stable in vacuum and aqueous phases[25,51,65,66] than thione form, and for this reason, it is not considered here. The physicochemical properties of the MBT molecule have been described in the literature[65–68]. Figure 3 shows the MBTH and MBT° forms. In order to better

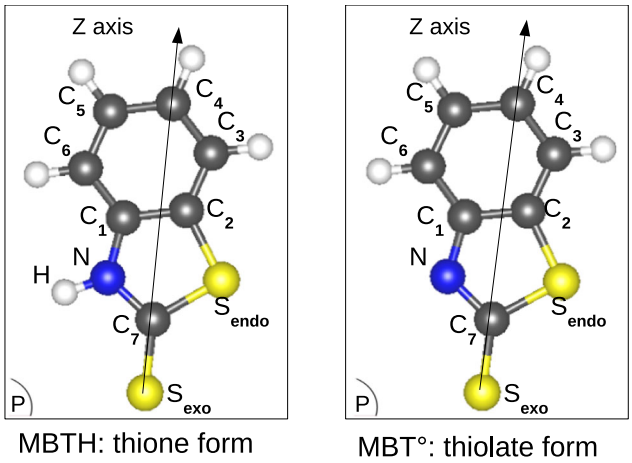

Fig. 3 MBT molecule under the thione (MBTH) and thiolate (MBT°) forms at isolated state. The Z axis passes through the S_{exo} and C_7 atoms.

describe the adsorption mode on the surface, we also represented the molecular plane and the Z axis of the molecule (axis joining the exocyclic S atom and the carbon C_7 atom). The orientation of the molecule with the surface is defined by the tilt angle of the Z axis and the molecular plane with respect to the surface plane.

In the present work, we focused on the formation of a full MBT (H) monolayer on the partially oxide-covered copper surface. We know from our previous study that a full MBT layer can form on oxidized copper surfaces with an intact oxide film, with a density of 3.27 molecule/nm^2. The supercell used was a 3×3 unit cell of the oxide, containing 9 MBT-adsorbed molecules. In the present work, the hole created in the oxide layer has an area, 0.305 nm^2, corresponding to that occupied by one molecule in the full organic monolayer on the oxide. By maintaining the number of 9 MBT molecules per supercell, the monolayer consists of six molecules adsorbed on each unsaturated Cu_{cus} site on the oxide surface and two molecules adsorbed on each unsaturated Cu_{cus} site of the oxide edges. The 9th molecule can be adsorbed on the oxide edge, the oxide wall, or on the metal at the bottom of the oxide hole. We envisaged these three configurations, studying for each one the most stable adsorption mode.

Since it was found from previous work that, at high coverage, both the thione and thiolate forms adsorb with their planes perpendicular to the surface, both on the bare metal surface[51] and on the fully oxide-covered surface[62], we did not consider the tilt and parallel orientations as starting configurations in the present work, but only the perpendicular orientation for the initial position of the molecules. Thus, MBT was initially oriented to the surface via the -S -S atoms or -S -N (NH) atoms.

The results obtained for the most relevant configurations are shown in Fig. 4 for the thione species and the adsorption of MBTH on each area of the partially oxidized copper surface is shown in Fig. 5. The snapshots in Fig. 5a, b correspond to the molecules adsorbed on the oxide surface and the snapshot in Fig. 5c to the molecules adsorbed on the oxide edges. They are similar for the configurations 1 and 2 in Fig. 4. The difference between the two configurations is in the adsorption of the 9th molecule shown in snapshot in Fig. 5d, e, where the 9th molecule is adsorbed on the metal surface in configuration 1 and on the oxide wall in configuration 2. The relevant adsorption configurations for the thiolate form are shown in Fig. 6 and the adsorption of MBT° on each area of the partially oxidized copper surface is shown in Fig. 7. The snapshot in Fig. 7a corresponds to the molecules adsorbed on the oxidized surface and the oxide edges, which is similar for all configurations in Fig. 6 and relates to eight molecules on the surface. The differences between the configurations 1–4 are

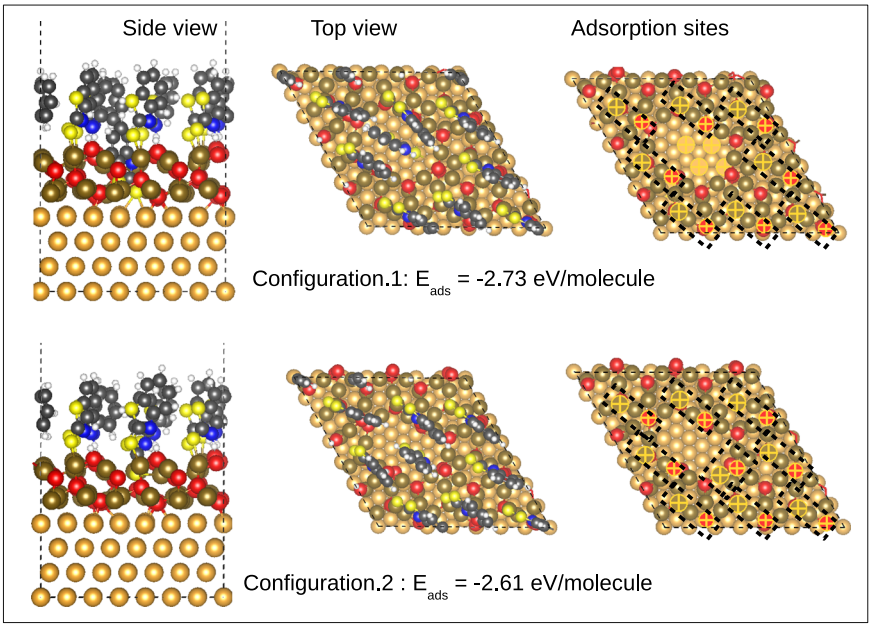

Fig. 4 Configurations 1 and 2 of MBTH form adsorbed on the partially oxide-covered copper surface. Illustration of side and top views and different adsorption sites on partially oxide-covered copper.

depicted in snapshots of Fig. 7b-e. They are for the 9th molecule. It is adsorbed on the metallic surface, in configurations 1 and 2 (snapshot in Fig. 7b, c), and on the oxide walls, in configurations 3 and 4 (Fig. 7d, e). The snapshots in Fig. 7b, c correspond to the molecule adsorbed on the metal surface via -S -S or via -S -N atoms, respectively, and the snapshots in Fig. 7d, e correspond to the molecule adsorbed on the oxide walls via -S atom or via -S -N atoms, respectively.

Table 1 compiles the adsorption energies of the thione and thiolate forms of MBT calculated by equation (1), for the most stable configurations. The negative values of the adsorption energy indicate that the adsorption process involving the different parts of the partially oxide-covered copper surface is an exothermic process. We calculated an adsorption energy of −2.73 and −2.61 eV/molecule for the configurations 1 and 2 of MBTH represented in Fig. 4. For MBT° in Fig. 6, the adsorption energies are −3.12 and −3.11 eV/molecule, for configurations 1 and 2, respectively, and −3.04 and −3.05 eV/molecule, for configurations 3 and 4, respectively. For both species, these adsorption energies are in the range of what we found for the interaction of MBT at the same coverage on the fully oxide-covered copper surface, for which the values were −2.71 and −3.11 eV/molecule for MBTH and MBT°, respectively[62]. However, the adsorption modes and the interaction mechanisms of the molecules are different and depend, in particular, on the different zones of the surfaces of the partially oxide-covered surface as illustrated by Fig. 1. Thus, a further step in the study was to understand the adsorption modes on each zone for both forms of the MBT molecule, and this is presented hereafter.

Adsorption on the oxide surface. On the oxide surface, the orientation of the adsorbed molecules is similar to that found on the fully oxide-covered surface for both MBT and MBT° forms. We recall that the molecule plane stands perpendicular to the surface and the -S -N (NH) atoms are directed toward the surface, which favors the formation of covalent and H-bonds between molecule and surface[62]. The -S -N orientation of the molecule toward the surface is more stable than -S -S orientation by 0.35 eV/molecule on oxidized copper surfaces with an intact oxide film[62]. The surface-relaxation effects on the oxidized copper surface with an intact oxide film have been described in our previous work[62]. Here, we observed similar behavior that the site symmetry is maintained when the molecules are adsorbed on the partially oxidized copper surface.

For MBTH adsorbed on the oxide surface of the partially oxide-covered system, there are two adsorption configurations. The first adsorption configuration, shown by the snapshot in Fig. 5a is identical to the adsorption of MBTH on oxidized copper surfaces with an intact oxide film[62]. The tilt angle of the Z axis is about 35°. MBTH is adsorbed in intact form and it binds covalently via the S_{exo} atom on top Cu_{cus} site and the bond length of S_{exo}–Cu_{cus} is 2.16 Å. The molecule forms also an H-bond via the NH group to O_{up} atoms. The distance of NH...O_{up} is in the range from 1.5 to 1.7 Å. Thus, the MBTH form adopted the orientation from Cu_{cus} to O_{up} on the oxide surface, which favors the formation of H-bonding. In this case, this requires that both Cu_{cus} and O_{up} sites are localized on the oxide surface.

The second configuration shown by the snapshot in Fig. 5b corresponds to MBTH adsorbed in the dissociative form by deprotonation of the NH group. The mechanism leads to the formation of an OH group on the oxide edge and the molecule gets into the thiolate form. This reaction is spontaneous and occurs without any activation energy. We observed this behavior only when the NH group of MBTH is directed toward an O^{*}_{up} atom, which misses two bonds with copper atoms and is localized on the oxide edge. Now, the Z axis of the molecule forms an angle of 30° with the surface. The adsorbed molecule forms an H-bond via the N atom and OH group and the distance N… HO^{*}_{up} is 1.68 Å. The molecule also forms covalent bond via the S_{exo} atom on top Cu_{cus} site. The S_{exo}–Cu_{cus} bond length is 2.16 Å. In this configuration, we can consider that the molecule is shared between the oxide surface and the oxide edge. This dissociative adsorption of MBTH contrasts with the first configuration and the results obtained on oxidized copper surfaces with an intact oxide film that showed that the dissociative adsorption of MBTH is not favored[62]. This also illustrates the presence on the surface of areas with acidic-site behavior (oxide surface) and others with basic-site behavior (oxide edges).

The MBT° species adsorbs via two covalent bonds on the oxide-covered surface (snapshot in Fig. 7a). It binds via the S_{exo} atom to Cu_{cus} and via the N atom to Cu_{csa}, with bond lengths of S_{exo}–Cu_{cus} and N–Cu_{csa} are 2.14 and 1.95 Å, respectively. The adopted orientation is from Cu_{cus} to Cu_{csa} on the oxide surface

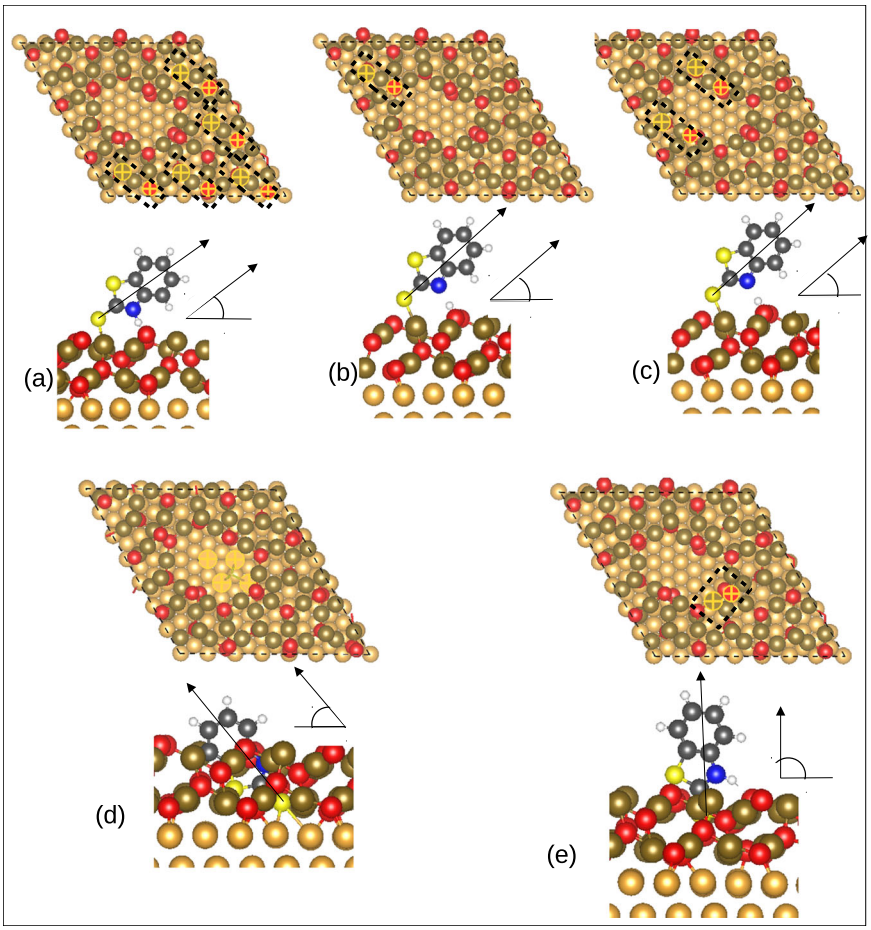

Fig. 5 Different snapshots of MBTH adsorbed on different parts of partially oxide-covered copper surface. a and **b** Illustrate adsorption of MBTH on the oxide surface, **c** on the oxide edges, **d** on metal surface (configuration 1), and **e** on the oxide wall (configuration 2).

and the Z axis tilted about 25° from the surface plane. This adsorption mode for MBT° on the oxide-surface part is in agreement with that found at similar coverage on oxidized copper surfaces with an intact oxide film[62].

Adsorption on the metal surface. For MBTH adsorbed on the metal surface at the bottom of the oxide hole, the most stable configuration, shown by the snapshot in Fig. 5d, is obtained with both sulfur atoms oriented toward the metal and the molecule plane oriented perpendicular to the surface plane. The Z axis of the molecule forms a tilt angle of 41° with the surface plane. Regarding the total energy difference (ΔE), the orientations via only -S or -S -N of the molecule toward the surface are less stable than the -S -S orientation by 0.22 and 0.29 eV, respectively. MBTH is adsorbed through the S_{exo} atom close to bridge site and the S_{endo} atom is localized on top site of copper metal surface. Indeed, the sulfur atoms can accommodate in hollow or bridge position at high coverage on the bare Cu(111) surface[51]. The bond lengths of S_{exo}–Cu are 2.40 and 2.34 Å close to the bridge site and the distance of S_{endo}–Cu is 3.01 Å on the top site. These results are consistent with those obtained on the oxide-free Cu(111) surface[51] that showed that the MBTH molecule in the most stable monolayer with a density of 3.9 molecule/nm^2 comprises two Cu–S bonds and is organized with a (3 × 3) superstructure. A similar adsorption mode was also found at lower density of 1.5 molecule/nm^2, however, with the two sulfur atoms of the molecule localized on a hollow hcp site like adsorbed atomic sulfur on Cu(111), whereas a mixed hollow and bridge position is reported at a coverage of 3.9 molecule/nm^2 [51].

MBT° is also adsorbed in a perpendicular orientation on the metal surface at the bottom of the oxide hole. However, the dehydrogenation of the MBT molecule makes the N site of the MBT° form more reactive. As a result, adsorbed MBT° can be oriented perpendicular via the -S -S atoms (Configuration 1 in Fig. 6 and snapshot in Fig. 7b) or via the -S -N atoms (Configuration 2 in Fig. 6 and snapshot in Fig. 7c) toward the metal surface. The Z axis of the molecule is tilted by 43° and 32°, respectively, from the surface plane. Regarding the total energy difference (ΔE), the adsorption of MBT° via the -S -S atoms is more stable by 0.11 eV than the adsorption via the -S -N atoms. However, the adsorption-energy difference (ΔE_{ads}) is only of 0.01 eV/molecule and reveals that both adsorption types are isoenergetic. For MBT° adsorbed on the oxide-free Cu(111) surface, a value of 0.10 eV was reported as adsorption-energy difference between the two configurations (-S -S and -S -N) at low molecular density (coverage of 1.5 molecule/nm^2) and the thiolate form makes two S–Cu bonds at high density (coverage of 3.9 molecule/nm^2) like the thione form[51]. In the present case, for -S–S-adsorption configuration, the S_{exo} and S_{endo} atoms are close to bridge and top copper metal sites, respectively. The bond lengths of S_{exo}–Cu are 2.30 and 2.38 Å and the bond length of S_{endo}–Cu is 2.75 Å. Whereas, for the -S -N adsorption configuration, the S_{exo} is located on the bridge site with the bond lengths S_{exo}–Cu of 2.28 and 2.46 Å on oxide-free Cu(111). At the bottom of the oxide hole, S_{exo} atom binds also covalently with the Cu_{csa} of the interfacial oxide plane, with a bond length S_{exo}–Cu_{csa} of 2.53 Å. The N atoms are located on the top site of a Cu metal atom and the bond length of N–Cu is 2.14 Å.

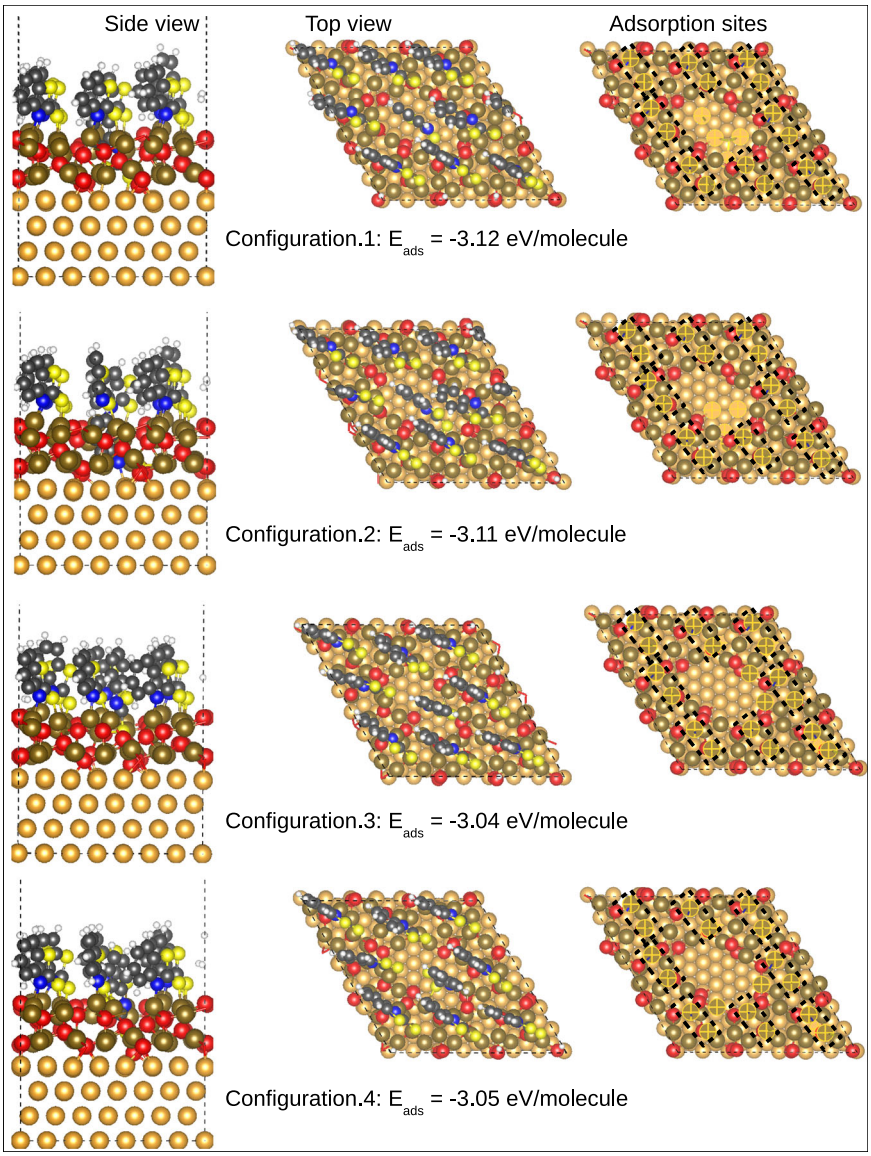

Fig. 6 Configurations from 1 to 4 of MBT° form adsorbed on the partially oxide-covered copper surface. Illustration of side and top views and different adsorption sites on partially oxide-covered copper.

Comparison of the interaction of MBT with the oxide-free copper surface reveals that MBT adsorbs more strongly on the fully oxidized copper surface[62] and on the partially oxidized copper surface than on the metal surface. Vernack et al.[51] reported an adsorption-energy value of −1.40 eV/molecule for the thione species on the Cu(111) surface at a coverage of 3.9 molecule/nm^2, where the molecules are oriented via -S -S toward the metal surface and sit on hollow and bridge sites. Geng et al.[69] reported that the adsorption of benzene thiolate on the fcc-bridge site of the (111) surface of metals, including Cu(111), is stronger via the S atom, with an adsorption energy of −2.26 eV/molecule

Adsorption on the oxide edges. For MBTH adsorbed at the edges of the oxide hole, as shown by the snapshot in Fig. 5c, the most stable configuration corresponds to the dissociative adsorption instead of intact molecular adsorption. We observed the proton transfer from the NH group to the oxygen localized on the oxide edges and this time the molecule binds via N..HO$^*_{up}$ H-bonding instead of NH...O$_{up}$ H-bonding observed on the oxide surface. The distance N...HO is 1.67 Å. The molecule also forms a covalent bond via the exocyclic sulfur atom on top of an unsaturated copper present on the oxide edges, with bond lengths of S$_{exo}$–Cu$_{cus}$ of 2.14 Å. This adsorption configuration of MBTH on the oxide edges is similar to the second configuration obtained for MBTH shared between the oxide and the oxide-edge parts (snapshots in Fig. 5b, c). We note that the dissociation process is spontaneous. The plane of the molecule is perpendicular to the surface and the Z axis is tilted by about 45° with respect to the surface plane.

The thiolate conformer adsorbed on the oxide edges (snapshot in Fig. 7a) adopts a similar adsorption configuration as on the oxide surface, with the molecule bonded via S$_{exo}$ to Cu$_{cus}$ and via N to Cu$_{csa}$. The molecular plane is perpendicular to the surface and the Z axis is tilted by about 25°. The bond lengths of S$_{exo}$–Cu$_{cus}$ and N–Cu$_{csa}$ are 2.12 and 1.96 Å, respectively.

Adsorption on the oxide walls. For the MBTH adsorbed at the walls of the oxide hole, as shown by the snapshot in Fig. 5e, the most stable configuration corresponds to the perpendicular orientation to the surface plane. However, MBTH is directed to the surface only via the exocyclic sulfur atom and the NH group is directed toward the

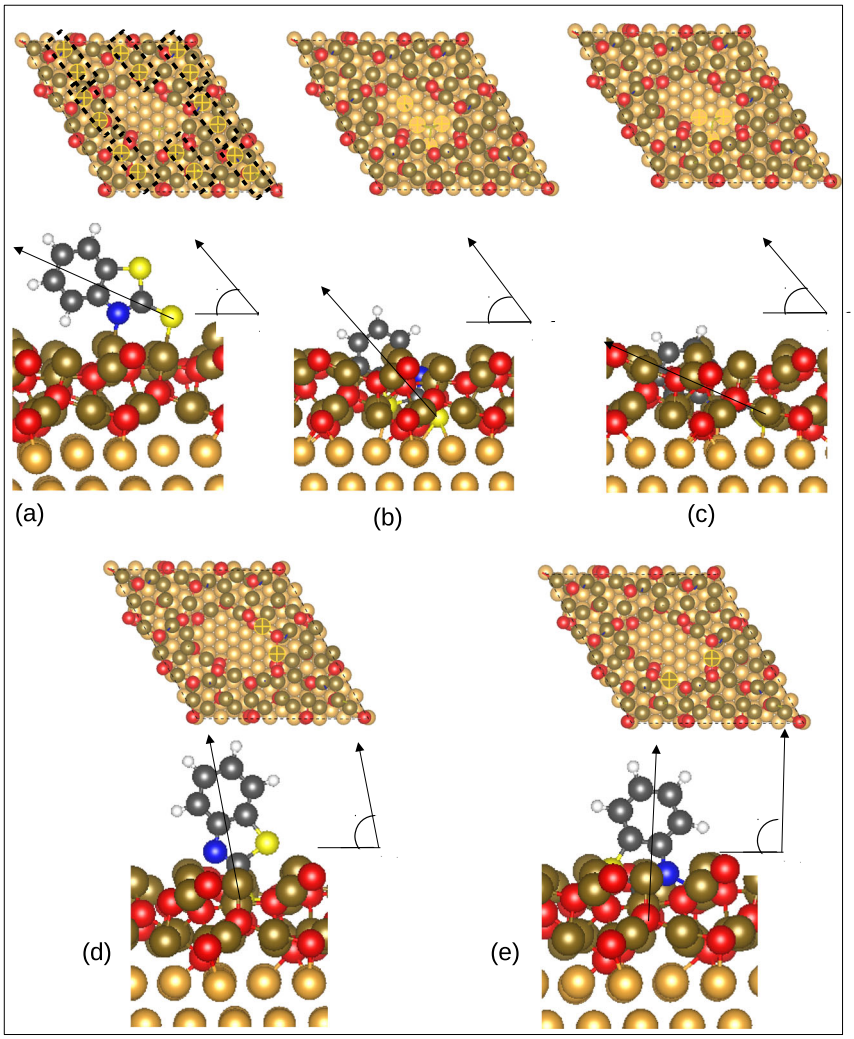

Fig. 7 Different snapshots of MBT° adsorbed on different parts of partially oxide-covered copper surface. a Illustrates the adsorption on the oxide surface and oxide edges, **b** and **c** on the metal surface (configurations 1 and 2), and **d** and **e** on the oxide walls (configurations 3 and 4).

Table 1. Adsorption energy (E_{ads} in eV/molecule) and total energy difference (ΔE_{total} in eV) of MBT for the thione (MBTH) and thiolate (MBT°) species adsorbed on the partially oxide-covered copper surface (Cu(111)||Cu_2O(111)-hole system). The adsorption energy is calculated using equation (1) for MBTH and MBT° forms.

MBT species	E_{ads} (eV/molecule)	ΔE_{total} (eV)	Fig.
MBTH	−2.73	0.00	Fig. 4 Conf.1
	−2.61	1.05	Fig. 4 Conf.2
MBT°	−3.12	0.00	Fig. 6 Conf.1
	−3.11	0.11	Fig. 6 Conf.2
	−3.05	0.76	Fig. 6 Conf.3
	−3.04	0.66	Fig. 6 Conf.4

oxide wall, which leads to the Z axis being perpendicular to the surface plane (tilt angle is almost 90°). In other words, the Z axis is parallel to the oxide-wall surface. The S_{exo} atom is localized at the distance of 4.17 Å from the metal surface, and thus not bonded to the metal Cu atoms. MBTH binds covalently via S_{exo} to Cu_{csa} with bond lengths of S_{exo}–Cu_{csa} of 2.44 Å. It also forms an H-bond via the NH group to an O_{up} surface atom with an NH...O_{up} distance of 1.79 Å.

For the MBT° conformer, the most stable configuration is with the plane of the molecule also perpendicular to the surface plane. The molecule is oriented toward the surface only via the S_{exo} atom and the N (or S_{endo}) atom is directed to the oxide wall like for adsorbed MBTH form. In this case also, the Z axis of the molecule is parallel to the oxide-wall surface. In configuration 3 in Fig. 6, the snapshot in Fig. 7d, MBT° forms two covalent bonds with the oxide wall via the S_{exo} to two Cu_{csa} sites at bond lengths of S_{exo}–Cu_{csa} of 2.22 and 2.47 Å. The Cu_{csa} sites involved in the formation of the covalent bond are localized on the oxide-wall surface. The S_{exo} atom is localized at a vertical distance of 3.96 Å from the metal surface and not bonded to metal Cu atoms. However, the deprotonation of the MBT allows the molecule to slide along the oxide-wall surface. Indeed, in another adsorption configuration (configuration 4 in Fig. 6, snapshot in Fig. 7e), the S_{exo} atom of the molecule is localized closer to the metal surface at the vertical distance of 2.80 Å. MBT° binds covalently via the S_{exo} and N atoms to Cu_{csa} sites at bond lengths of S_{exo}–Cu_{csa} and N–Cu_{csa} of 2.42 and 2.03 Å, respectively. The Cu_{csa} sites involved in the covalent bonding are localized on the oxide-wall surface. The two configurations have similar adsorption energy (ΔE_{ads} = 0.01 eV) and we calculated a total energy difference (ΔE) of 0.10 eV. This indicates that these two adsorption modes of thiolate on the oxide walls are isoenergetic.

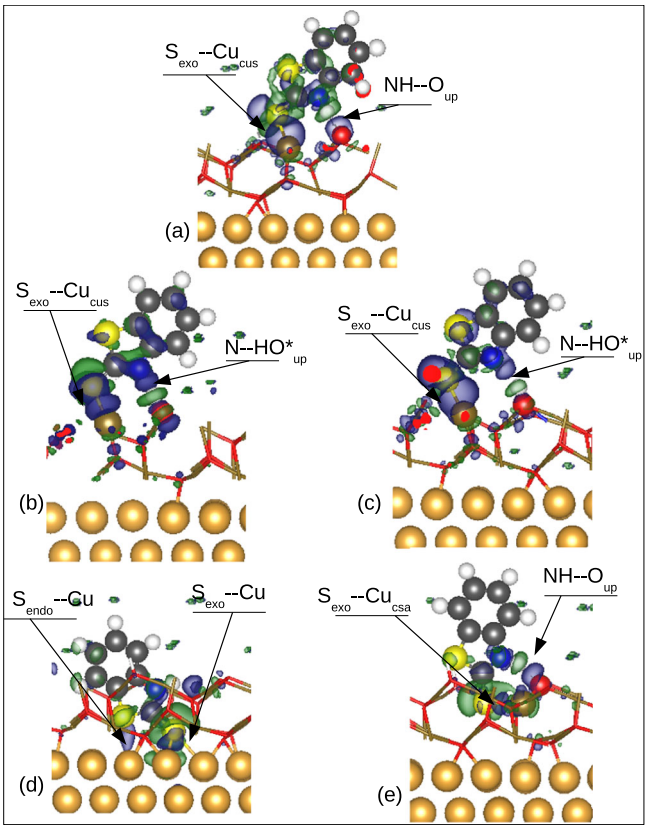

Fig. 8 Charge-density difference analysis for MBTH adsorbed on partially oxide-covered copper surface. a and **b** Snapshots on the oxide surface, **c** on the oxide edges, **d** on the metal surface, and **e** on the oxide wall. Light blue and green colors of isosurface correspond to accumulation and depletion of charge density, respectively.

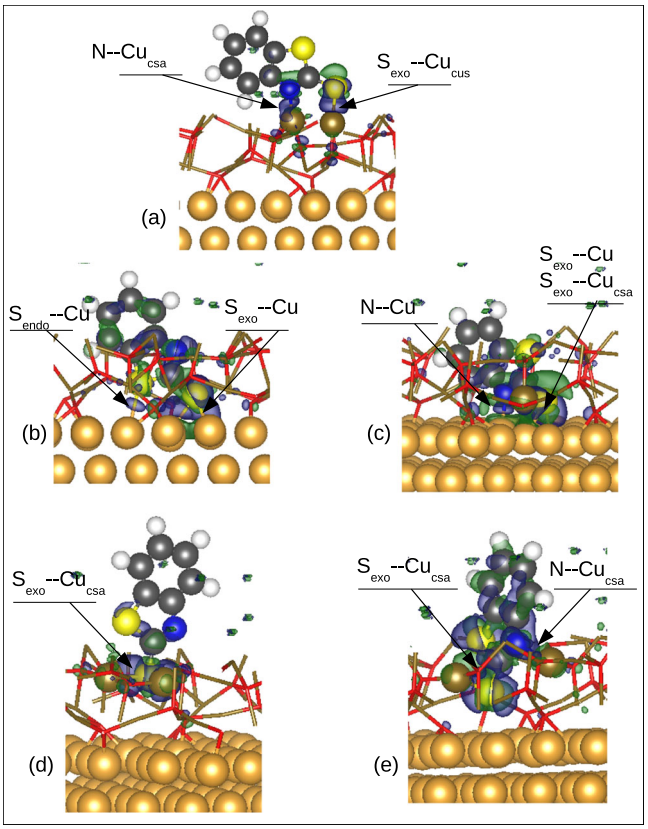

Fig. 9 Charge-density difference analysis for MBT° adsorbed on partially oxide-covered copper surface. a Snapshot on the oxide surface and oxide edges, **b** and **c** on the metal surface, and **d** and **e** on the oxide walls. Light blue and green colors of the isosurface correspond to accumulation and depletion of charge density, respectively.

Electronic analysis of MBT adsorbed on the partially oxide-covered copper surface

In order to provide more details on the molecule-surface interaction, we analyzed the charge density difference ($\Delta\rho(r)$), using equation (3). Figures 8 and 9 show the charge-density difference for MBT thione and thiolate species, respectively, adsorbed on the different parts of the partially oxide-covered surface. For better visualization of the isosurface, we represented the charge-density difference of only one molecule for each adsorption mode and plotted with an isosurface of ± 0.0004 e/Å^3 and ± 0.0009 e/Å^3 for the thione and thiolate species, respectively.

Figure 8a and b shows the charge density difference of MBTH adsorbed on the oxide surface, and Fig. 8c on the oxide edges. The strength of the bonding of the molecule to the surface is confirmed by the formation of covalent and H bonds. The charge-density accumulation (light-blue color) between the S_{exo} and Cu_{cus} atoms corresponds to the formation of a S_{exo}-Cu_{cus} covalent bond. NH...O_{up} H-bonding is confirmed by the charge-density accumulation on the O_{up} atom and charge-density depletion (green color) on the hydrogen atom of the NH group. The dissociative adsorption of MBTH is also confirmed by charge-density analysis in Fig. 8b and c which shows charge-density accumulation on the N atom and charge-density depletion on the hydrogen atom adsorbed on O^*_{up}, localized at the oxide edge. This confirms $N\cdots HO^*_{up}$ H-bonding.

On the metal at the bottom of the oxide holes, the MBTH conformer interacts via both sulfur (-S -S) atoms, as observed in Fig. 8d, by the charge-density accumulation and depletion on the sulfur atoms and metal copper-surface atoms, respectively.

In Fig. 8e, the strong interaction of MBTH with the oxide walls is confirmed. Indeed, we observe charge-density accumulation (light-blue color) and depletion (green color) on the S_{exo} and Cu_{csa} atoms, respectively, confirming the S_{exo}–Cu_{csa} covalent bonding. The charge-density accumulation on the O_{up} atom and the charge density depletion on the hydrogen atom of the NH group also confirms the NH...O_{up} H-bonding.

Figure 9a corresponds to MBT° adsorbed on the oxide surface and on the oxide edges. The analysis confirms again the strength of the adsorption on both parts by the formation of S–Cu_{cus} and N–Cu_{csa} covalent bonds. We recall that both parts show similar adsorption configurations of MBT°.

Figure 9b, c corresponds to MBT° adsorbed on the metal surface at the bottom of the oxide holes by -S -S atoms and by -S -N atoms, respectively. They show charge density accumulation and depletion on different atoms involved in the formation of covalent bonds between the molecule and the metal surface. In addition, a charge-density accumulation and depletion is observed on the S_{exo} atom and the Cu_{csa} atom localized on the oxide wall (Fig. 9c). Again, these results confirm the strong interaction of MBT° with the metal surface by the formation of S–Cu and N–Cu covalent bonds.

Figure 9d, e confirms strong adsorption also on the oxide walls. In Fig. 9d, the molecule MBT° interacts via the S_{exo} atom to Cu_{csa}, which is confirmed by the charge-density accumulation and depletion on these two atoms. In Fig. 9e, the respective charge-density accumulation and depletion on the S_{exo} and Cu_{csa} atoms and on the N and Cu_{csa} atoms confirm again the formation of S_{exo}–Cu_{csa} and N–Cu_{csa} covalent bonds.

Table 2. Bader charge analysis for MBTH and MBT° species. ΔQ_{mol}, ΔQ_{oxide} and ΔQ_{metal} correspond to the Bader charge analysis on the molecule, oxide and the metal, respectively, in electron/molecule.

MBT species	ΔQ_{mol}	ΔQ_{oxide}	ΔQ_{metal}
MBTH	$+0.15 \pm 0.05$	-0.16 ± 0.01	± 0.02
MBT°	-0.37 ± 0.03	$+0.30 \pm 0.02$	$+0.07 \pm 0.03$

Table 2 summarizes the Bader charge analysis calculated by equation (4) for MBTH and MBT° adsorbed on different areas of the partially oxide-covered copper surface.

For MBTH, the Bader charge analysis reveals an electron transfer from the organic layer to the oxide. Each molecule loses an average of 0.15 ± 0.05 electron. However, when MBTH is adsorbed intact on the metal and the oxide parts, the electron transfer is slightly higher than for dissociative adsorption by 0.05 electron. The gain of electrons is localized in the oxide part ($\Delta Q = 0.16 \pm 0.01$ electron/molecule). We note that the copper metal atoms show no significant change after adsorption ($\Delta Q < \pm 0.02$ electron/molecule). Despite the molecule losing electronic charge, the S_{exo} atom in the molecule is charged negatively, regardless of the adsorption site. The electrons come from the redistribution of the electrons on the molecule. The S_{exo} atom gains from 0.10 to 0.15 electron and from 0.20 to 0.25 electron for the intact and dissociative adsorption configurations, respectively.

In contrast, the Bader charge analysis for MBT° reveals that the molecules in the organic layer gain electrons coming from the substrate. Each molecule gains an average of 0.37 ± 0.03 electron. As found in our previous works on the metal surface[51] and on the oxide-covered metal[62], the final state of MBT is anionic even starting from MBT°, confirming that the MBT dissociation at the surface is heterolytic. Most of the charge, 0.30 ± 0.02 electron/molecule, comes from the oxide part of the substrate, and only 0.07 ± 0.01 electron/molecule from the metal part. The S_{exo} atom in the molecule is again charged negatively and it gains from 0.23 to 0.34 electron.

DISCUSSION

Our results show that the partially oxide-covered copper surface contains different sites susceptible to interact with the organic inhibitor. The most reactive sites are Cu_{cus}, Cu_{csa}, and O_{up} on the oxide surface, Cu_{cus}, Cu_{csa}, and O^*_{up} on the oxide edges, Cu_{csa} on the oxide walls and Cu on the metal at the bottom of the oxide holes. For both forms of MBT molecule, the exocyclic sulfur atom remains the most reactive site, whatever the reacting part of the partially oxide-covered copper surface. In addition, the NH group or N atom and endocyclic sulfur atom can be involved in the adsorption process, depending on the adsorption conformers and the adsorption zones.

To summarize, MBTH forms an S_{exo}-Cu_{cus} covalent bond with an NH...O_{up} or N...HO^*_{up} H-bond on the oxide surface and the oxide edges, an S_{exo}-Cu_{csa} covalent bond and an NH...O_{up} H-bond on the oxide walls, and S_{exo}–Cu and S_{endo}–Cu covalent bonds on the metal surface. The adsorption mechanism involving the formation of NH...O_{up} and N...HO^*_{up} H-bonds corresponds to the intact and dissociative adsorption modes, respectively. The intact adsorption of the molecule occurs when an unsaturated oxygen (O_{up}) is present, while the dissociative adsorption occurs spontaneously in the presence of doubly unsaturated oxygen (O^*_{up}), present at the oxide edges. In contrast, MBT° favors the formation of two covalent bonds, which increases its bonding to the substrate as compared with MBTH. MBT° forms S_{exo}–Cu_{cus} and N–Cu_{csa} covalent bonds on the oxide surface and the oxide edges and an S_{exo}-Cu_{csa} and N–Cu_{csa} or only S_{exo}–Cu_{csa} covalent bonds on the oxide walls. MBT° binds also covalently on the metal surface via an S_{exo}-Cu and N–Cu or an S_{exo}-Cu. We found that the formation of N–Cu or S_{endo}–Cu is isoenergetic on the metal surface.

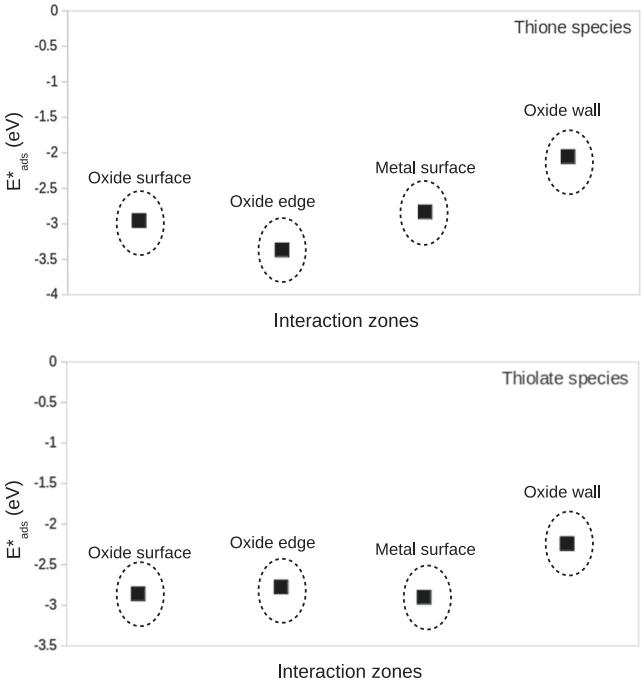

Fig. 10 Local energetic trends. Thione and thiolate species adsorbed on the different surface zones on a partially oxide-covered copper surface.

It is well known that the factors determining the efficiency of organic inhibitors against the corrosion of metals are related to their ability to form protective films, and depend on adsorption energy and bonding strength on metal surfaces. Previously, we demonstrated by quantum chemical DFT calculations that the MBT molecule interacts strongly and forms well-ordered and dense organic layers on both bare (oxide-free) and fully oxide-covered copper surfaces[51,62]. Here, we show that the adsorption of MBT at high coverage under thione and thiolate forms is also an exothermic process on the partially oxide-covered copper surface. Our energetic analysis, based on the adsorption energy calculated by equation (1), also shows the ability of MBT to form a strongly adsorbed organic film like on the oxide-free and fully oxide-covered copper surface. However, as the partially oxide-covered copper surface consists of different local parts, which present different reactive sites, it is interesting to discuss the local energetic trends, in order to identify on which type of surface the MBT molecule can interact in priority.

To do that, we used equation (2) to calculate the adsorption energy of one molecule on each zone. The protocol was to start from the surface fully covered by the organic monolayer (nine molecules per supercell) and to remove one molecule from each part of interest of the partially oxide-covered copper surface (eight molecules per supercell). We applied this protocol to all the different configurations of MBTH and MBT° forms discussed above. This allowed, by simple energy comparison, to identify the most reactive parts of the surface.

Figure 10 shows the adsorption-energy values for MBTH and MBT° on different parts of the partially oxide-covered copper surface. Both forms of MBT interact strongly with the different areas, however, the local reactivity and the order of the adsorption depend on the surface type.

Oxide edges are the most reactive local surfaces with an average energy of 3.38 eV for MBTH adsorbed in dissociative form.

This high reactivity of the oxide edges is due to the combined presence of both the unsaturated copper and doubly unsaturated oxygen sites. Thus, the molecule can be expected to block these sites that are susceptible to interact with aggressive ions, like chloride ions, and thus are highly sensitive to corrosion. The second most reactive part is the oxide surface, which contains the unsaturated copper and oxygen sites, with an energy of −3.05 eV. In this case, the presence of the molecule on the oxide surface enhances the barrier properties of the oxide film. The third most reactive local part is the metal surface with an energy of −2.83 eV for MBTH. The adsorption of MBTH can thus protect the metal surface from interaction with the environment in the locally depassivated areas where the oxide has been removed. Note that this energy is significantly higher than that calculated for a plain MBT SAM on Cu(111), −1.4 eV/molecule[51]. In contrast, MBT° presents similar reactivity toward the oxide surface, oxide edges, and metal-surface local parts, with energies ranging from −2.75 to −2.90 eV, showing thus no local hierarchy between these three types of surface. Both for MBTH and MBT°, oxide walls present the lowest reactivity, which is because it contains only saturated copper sites. The interaction energies of MBTH and MBT° on the oxide walls are −2.05 and −2.24 eV, respectively. Despite being the least reactive toward the inhibitor molecule, the interactions energies show that the adsorption of MBT molecule on the oxide walls, combined with adsorption of the oxide edges, can be expected to slow down the dissolution of the oxide and the enlargement of the depassivated areas. Besides, the present study shows that when low coordinated Cu and O sites are exposed, they are the favored sites for adsorption. Thus, the inhibition will increase when the oxide wall orientation is a nanofacet with a high density of low coordinated sites.

The construction of an original model of copper partially covered by an ultrathin copper oxide film enabled the study of the bonding mechanisms, energetic trends, stability, and electronic properties of the MBT-corrosion inhibitor adsorbed on the different parts of an incompletely passivated surface (or locally depassivated) by means of DFT quantum chemical calculations.

The results show the ability of the MBT molecule to form a strongly adsorbed organic film on the oxide-covered copper surface, whatever the thione or thiolate forms and the surface zones. However, differences in the adsorption mechanisms and the bonding strength are evidenced between the forms of MBT and the considered local surface.

The reactive surface sites are the coordinatively unsaturated (Cu_{cus}), coordinatively saturated (Cu_{csa}) Cu atoms of the oxide, Cu atoms of the metal, and unsaturated (O_{up}) and doubly unsaturated (O^*_{up}) oxygen atoms of the oxide, according to the local nature of the surface. In the MBT molecule, the S_{exo} atom is the most reactive site and the molecule can also interact via the S_{endo} or N atoms or the NH group, according to the adsorbed conformer.

MBTH can form one covalent bond by S_{exo}–Cu_{cus} on the oxide edges and oxide surface or by S_{exo}–Cu_{csa} on the oxide walls, in addition to one NH...O_{up} or N...HO^*_{up} H-bond in the intact or dissociative adsorption, respectively. Dissociative adsorption is promoted by the doubly unsaturated O^*_{up} sites at the oxide edges. On the metal surface, MBTH can chemically bond via both S_{exo} and S_{endo} to Cu atoms. Decreasing order of local adsorption strength is as follows: oxide edges > oxide surface > metal surface > oxide walls.

MBT° can form two covalent bonds by S_{exo}–Cu_{cus} and N–Cu_{csa} on the oxide edges and on the oxide surface or by S_{exo}–Cu_{csa} and N–Cu_{csa} on the oxide walls. On the metal surface, it can chemically bond by S_{exo}–Cu and N–Cu or by both S atoms. The order of local adsorption strength is oxide edges = oxide surface = metal surface > oxide walls.

The strong interaction of the MBT molecule on different local parts of the partially oxidized copper surface reveals its ability to block the initiation of localized corrosion (pitting) and to protect depassivated (or incompletely passivated) areas by mitigating the dissolution of both the oxide and the bare metal.

METHODS

Computational details

All calculations were performed by applying the framework of DFT with the periodic plane-wave basis set implemented in Vienna Ab initio Simulation Package (VASP)[70–73]. All results reported have been obtained with projector-augmented wave potentials using a 450 eV plane wave cutoff[74,75]. Electron exchange and correlation terms were treated within the generalized gradient approximation (GGA) of Perdew–Burke–Ernzehof (PBE) functional[76,77]. We used a Methfessel–Paxton smearing[78] with smearing value of 0.1 eV. Because of the large unit-cell size used in calculations, the Brillouin zone sampling was restricted to the Γ-point[79]. van der Waals contributions were considered in the local van der Waals density-functional scheme proposed by Dion et al.[80] and Klimeš et al.[81–83] and calculations were carried out using OptB86b-vdw level[82], offering a good compromise for the lattice parameters of bulk Cu metal and Cu_2O oxide with equilibrium values of 3.599 (–0.30%) and 4.272 Å (+0.05%), in good agreement with experimental values of 3.61[84] and 4.27 Å[85], respectively. Atomic positions were relaxed with the conjugate-gradient (CG) algorithm, until forces on each moving atom were less than 0.02 $eVÅ^{-1}$. The oxide layer and the atoms from the molecules were let free to relax. All calculations are done without any constraint on the structure, except the two bottom layers of the metals (asymmetric slab).

Energy analysis

The adsorption energy of the MBT molecule under thione (MBTH) and thiolate (MBT°) forms was calculated as

$$E_{\mathrm{ads}} = [E(\,\mathrm{slab/MBT}) - E(\mathrm{slab}) - nE(\mathrm{MBT}\,)]/n \quad (1)$$

where E(slab/MBT) is the total energy of the system with MBTH or MBT° adsorbed on the slab surface. E(slab) and E(MBT) are the energies of the bare, relaxed Cu(111)||Cu_2O(111) slab and the free MBTH or MBT° molecule optimized in vacuum, respectively. n is the number of molecules on the surface. MBT is more likely to be present in the anionic form rather than as a radical in aqueous solution. However, here we compare different adsorption configurations and adsorption sites for the same molecular state, and the ranking in energy will not be modified by adding the anionization free energy of MBT.

When two configurations i and j are energetically compared, we use the total energy difference $\Delta E = E(i) - E\ (j)$ as well as the average energy difference (per molecule) $\Delta E_{ads} = E_{ads}(i) - E_{ads}(j)$, where E($i$) and E($j$) are the total energies, and $E_{ads}(i)$ and $E_{ads}(j)$ are the average adsorption energies of configurations i and j, respectively.

In order to estimate the reactivity of different parts of the partially oxide-covered copper surface toward the MBT molecule, we calculated the energy trends of MBT on different surface zones as:

$$E^*_{\mathrm{ads}} = -(E(slab/MBT_{n-1}) + E(MBT) - E(slab/MBT_n)) \quad (2)$$

where E(slab/MBT_n) and E(slab/MBT_{n-1}) correspond to the total energy of the n and $(n-1)$ molecules adsorbed on the slab surface, respectively.

Electronic analysis

We plotted the charge-density difference expressed as follows:

$$\Delta\rho(r) = \rho(r)_{\mathrm{slab/mol}} - (\rho(r)_{\mathrm{slab}} + \rho(r)_{\mathrm{mol}}) \quad (3)$$

where $\rho(r)_{\mathrm{slab/mol}}$ is the charge-density distribution on the adsorbed system. $\rho(r)_{\mathrm{slab}}$ and $\rho(r)_{\mathrm{mol}}$ are the charge-density distributions on the isolated slab and the molecule for the geometry after adsorption, respectively.

The net charge variation was determined on each atom by

$$\Delta Q(x) = Q_{\mathrm{ads}}(x) - Q_{\mathrm{vac}}(x) \quad (4)$$

where $Q_{\mathrm{ads}}(x)$ and $Q_{\mathrm{vac}}(x)$ are the net charges on each atom (Bader population analysis)[86] of the adsorbed and free molecule, respectively.

DATA AVAILABILITY

The data that support the finding of this study are available from the corresponding authors upon reasonable request.

Received: 9 February 2021; Accepted: 20 May 2021;
Published online: 30 September 2021

REFERENCES

1. Twite, R. L. & Bierwagen, G. P. Review of alternatives to chromate for corrosion protection of aluminum aerospace alloys. *Prog. Org. Coat.* **33**, 91–100 (1998).
2. Raja, P. B. & Sethuraman, M. G. Natural products as corrosion inhibitor for metals in corrosive media - A review,. *Mater. Lett.* **62**, 113–116 (2008).
3. Gangopadhyay, S. & Mahanwar, P. A. Recent developments in the volatile corrosion inhibitor (VCI) coatings for metal: a review. *J. Coat. Technol. Res.* **15**, 789–807 (2018).
4. Milošev, I. Contemporary modes of corrosion protection and functionalization of materials. *Acta Chim. Slov.* **66**, 511–533 (2019).
5. Maurice, V. & Marcus, P. Progress in corrosion science at atomic and nanometric scales. *Prog. Mater. Sci.* **95**, 132–171 (2018).
6. Chiter, F., Lacaze-Dufaure, C., Tang, H. & Pébére, N. DFT studies of the bonding mechanism of 8-hydroxyquinoline and derivatives on the (111) aluminum surface. *Phys. Chem. Chem. Phys.* **17**, 22243 (2015).
7. Chiter, F., Bonnet, M.-L., Lacaze-Dufaure, C., Tang, H. & Pébére, N. Corrosion protection of Al(111) by 8-hydroxyquinoline: a comprehensive DFT study. *Phys. Chem. Chem. Phys.* **20**, 21474 (2018).
8. Kokalj, A. & Peljhan, S. Density functional theory study of adsorption of benzotriazole on Cu_2O surfaces. *J. Phys. Chem. C* **119**, 11625–11635 (2015).
9. Kokalj, A., Gustinčič, D., Poberžnik, M. & Lozinšek, M. New insights into adsorption bonding of imidazole: a viable C2-H bond cleavage on copper surfaces. *Appl. Surf. Sci.* **479**, 463–468 (2019).
10. Denissen, P. J. & Garcia, S. J. Reducing subjectivity in EIS interpretation of corrosion and corrosion inhibition processes by in-situ optical analysis. *Electrochim. Acta* **293**, 514–524 (2019).
11. Xhanari, K. & Finšgar, M. The corrosion inhibition of AA6082 aluminium alloy by certain azoles in chloride solution: Electrochemistry and surface analysis. *Coating* **9**, 380 (2019).
12. Zadeh, M. A., Tedim, J., Zheludkevich, M., van der Zwaag, S. & Garcia, S. J. Synergetic active corrosion protection of AA2024-T3 by 2D- anionic and 3D-cationic nanocontainers loaded with Ce and mercaptobenzothiazole. *Corros. Sci.* **135**, 35–45 (2018).
13. Visser, P., Terryn, H. & Mol, J. M. C. On the importance of irreversibility of corrosion inhibitors for active coating protection of AA2024-T3. *Corros. Sci.* **140**, 272–285 (2018).
14. Balaskas, A. C., Hashimoto, T., Curioni, M. & Thompson, G. E. Two-shell structured PMAA@CeO_2 nanocontainers loaded with 2-mercaptobenzothiazole for corrosion protection of damaged epoxy coated AA2024-T3. *Nanoscale* **9**, 5499 (2017).
15. Maia., F. et al. Corrosion protection of AA2024 by sol-gel coatings modified with MBT-loaded polyurea microcapsules. *Chem. Eng. J.* **283**, 1108–1117 (2016).
16. Roussi, E., Tsetsekou, A., Skarmoutsou, A., Charitidis, C. A. & Karantonis, A. Anticorrosion and nanomechanical performance of hybrid organo-silicate coatings integrating corrosion inhibitors. *Surf. Coat. Techn.* **232**, 131–141 (2013).
17. Liu, D., Han, E., Song, Y. & Shan, D. Enhancing the self-healing property by adding the synergetic corrosion inhibitors of Na_3PO_4 and 2-mercaptobenzothiazole into the coating of Mg alloy. *Electrochim. Acta* **323**, 134796 (2019).
18. Xie, Z.-H. & Shan, S. Nanocontainers-enhanced self-healing Ni coating for corrosion protection of Mg alloy. *J. Mater. Sci.* **53**, 3744–3755 (2018).
19. Cen, H., Cao, J., Chen, Z. & Guo, X. 2-mercaptobenzothiazole as a corrosion inhibitor for carbon steel in supercritical CO_2-H_2O condition. *Appl. Surf. Sci.* **476**, 422–434 (2019).
20. Mirzakhanzadeh, Z. et al. Enhanced corrosion protection of mild steel by the synergetic effect of zinc aluminum polyphosphate and 2-mercaptobenzimidazole inhibitors incorporated in epoxy-polyamide coatings. *Corros. Sci.* **138**, 372–379 (2018).
21. Kartsonakis, I. A. et al. A comparative study of corrosion inhibitors on hot-dip galvanized steel. *Corros. Sci.* **112**, 289–307 (2016).
22. Rahmani, K., Jadidian, R. & Haghtalab, S. Evaluation of inhibitors and biocides on the corrosion, scaling and biofouling control of carbon steel and copper-nickel alloys in a power plant cooling water system. *Desalination* **393**, 174–185 (2016).
23. Gholami, M., Danaee, I., Maddahy, M. H. & RashvandAvei, M. Correlated ab initio and electroanalytical study on inhibition behavior of 2-mercaptobenzothiazole and its thiole thione tautomerism effect for the corrosion of steel (API 5L X52) in sulphuric acid solution. *Ind. Eng. Chem. Res.* **52**, 14875–14889 (2013).
24. Zhang, J., Zhang, Q., Ren, H., Zhao, W. & Zhang, H. Inhibition performance of 2-mercaptobenzothiazole derivatives in CO_2 saturated solution and its adsorption behavior at Fe surface. *Appl. Surf. Sci.* **253**, 7416–7422 (2017).
25. Li, Y. et al. The corrosion and lubrication properties of 2-mercaptobenzothiazole functionalized ionic liquids for bronze. *Tribol. Int.* **114**, 121–131 (2017).
26. Xing, X., Xu, X., Wang, J. & Hu, W. Preparation, release and anticorrosion behavior of a multi-corrosion inhibitors-halloysite nanocomposite. *Chem. Phys. Lett.* **718**, 69–73 (2019).
27. Woods, R., Hope, G. A. & Watling, K. A SERS spectroelectrochemical investigation of the interaction of 2-mercaptobenzothiazole with copper, silver and gold surfaces. *J. Appl. Electrochem.* **30**, 1209–1222 (2000).
28. Grekulović, V., Vujasinović, M. R. & Mitovski, A. Electrochemical behavior of AgCu50 in alkaline media in the presence of clorides and 2-mercaptobenzothiazole. *J. Min. Metall. Sect. B-Metall* **53**, 349–356 (2017).
29. Yang, H. et al. 2-mercaptobenzothiazole monolayers on zinc and silver surfaces for anticorrosion. *Corros. Sci.* **50**, 3160–3167 (2008).
30. Cui, B., Chen, T., Wang, D. & Wan, L.-J. In situ STM evidence for the adsorption geometry of three n-heteroaromatic thiols on Au(111). *Langmuir* **27**, 7614–7619 (2011).
31. Shervedani, R. K. & Babadi, M. K. Application of 2-mercaptobenzothiazole self-assembled monolayer on polycrystalline gold electrode as a nanosensor for determination of Ag(I). *Talanta* **69**, 741–746 (2006).
32. Bharathi, S., Yegnaraman, V. & Rao, G. P. Potential-dependent "opening" and "closing" of self-assembled 2-mercaptobenzthiazole on gold substrates. *Langmuir* **9**, 1614–1617 (1993).
33. Ohsawa, M. & Suetaka, W. Spectro-electrochemical studies of the corrosion inhibittion of copper by 2-mercaptobenzothiazole. *Corros. Sci.* **19**, 709–722 (1979).
34. Chadwick, D. & Hashemi, T. Electron spectroscopy of corrosion inhibitors: Surface films formed by 2-mercaptobenzothiazole and 2-mercaptobenzimidazole on copper. *Surf. Sci.* **89**, 649–659 (1979).
35. Marconato, J. C. & Bulho, L. O. A spectroelectrochemical study of the inhibition of the electrode process on copper by 2- mercaptobenzothiazole in ethanolic solutions. *Electrochim. Acta* **43**, 771–780 (1998).
36. Ramírez-Cano, J. A., Veleva, L., Souto, R. M. & Fernández-Pérez, B. M. SECM study of the pH distribution over Cu samples treated with 2-mercaptobenzothiazole in NaCl solution. *Electrochem. commun.* **78**, 60–63 (2017).
37. He, D., Chen, F., Chen, J., Yao, S. & Wei, W. Real-time bulk acoustic wave studies of the inhibition behavior of mercaptobenzothiazole on copper. *Thin Solid Films* **352**, 234–238 (1999).
38. Finšgar, M. & Merl, D. K. An electrochemical, long-term immersion, and XPS study of 2-mercaptobenzothiazole as a copper corrosion inhibitor in chloride solution. *Corros. Sci.* **83**, 164–175 (2014).
39. Shahrabi, T., Tavakholi, H. & Hosseini, M. G. Corrosion inhibition of copper in sulphuric acid by some nitrogen heterocyclic compounds. *Anti-Corros. Method. M.* **54**, 308–313 (2007).
40. Bao, Q., Zhang, D. & Wan, Y. 2-mercaptobenzothiazole doped chitosan/11-alkanethiolate acid composite coating: Dual function for copper protection. *Appl. Surf. Sci.* **257**, 10529–10534 (2011).
41. Kazansky, L. P., Selyaninov, I. A. & Kuznetsov, Y. I. Adsorption of 2-mercaptobenzothiazole on copper surface from phosphate solutions. *Appl. Surf. Sci.* **258**, 6807–6813 (2012).
42. Chen, Y.-H. & Erbe, A. The multiple roles of an organic corrosion inhibitor on copper investigated by a combination of electrochemistry-coupled optical in situ spectroscopies. *Corros. Sci.* **145**, 232–238 (2018).
43. Wu, X., Wiame, F., Maurice, V. & Marcus, P. Adsorption and thermal stability of 2-mercaptobenzothiazole corrosion inhibitor on metallic and pre-oxidized Cu (111) model surfaces. *Appl. Surf. Sci.* **508**, 145132 (2020).
44. Wu, X., Wiame, F., Maurice, V. & Marcus, P. 2-mercaptobenzothiazole corrosion inhibitor deposited at ultra-low pressure on model copper surfaces. *Corros. Sci.* **166**, 108464 (2020).
45. Gründer, Y. et al. Structure and electrocompression of chloride adlayers on Cu (111). *Surf. Sci.* **605**, 1732–1737 (2011).
46. Gründer, Y. et al. Cu(111) in chloride containing acidic electrolytes: Coadsorption of an oxygenated species. *J. Electroanal. Chem.* **712**, 74–81 (2014).
47. Baricuatro, J. H. et al. Structure and composition of Cu(hkl) surfaces exposed to O_2 and emersed from alkaline solutions: Prelude to UHV-EC studies of CO_2 reduction at well-defined copper catalysts. *J. Electroanal. Chem.* **716**, 101–105 (2014).
48. Maurice, V., Strehblow, H.-H. & Marcus, P. In situ STM study of the initial stages of oxidation of Cu(111) in aqueous solution. *Surf. Sci.* **458**, 185–194 (2000).
49. Abrahami, S. T. et al. In situ EC-STM study and DFT modeling of the adsorption of glycerol on Cu(111) in NaOH solution. *J. Phys. Chem. C* **123**, 22228–22238 (2019).
50. Zhang, Z., Wang, Q., Wang, X. & Gao, L. The influence of crystal faces on corrosion behavior of copper surface: First-principle and experiment study. *Appl. Surf. Sci.* **396**, 746–753 (2017).
51. Vernack, E., Costa, D., Tingaut, P. & Marcus, P. DFT studies of 2-mercaptobenzothiazole and 2-mercaptobenzimidazole as corrosion inhibitors for copper. *Corros. Sci.* **174**, 108840 (2020).

52. Gustinčič, D. & Kokalj, A. DFT study of azole corrosion inhibitors on Cu_2O model of oxidized copper surfaces: I. Molecule-surface and Cl-surface bonding. *Metals* **8**, 310 (2018).
53. Gustinčič, D. & Kokalj, A. DFT study of azole corrosion inhibitors on Cu_2O model of oxidized copper surfaces: II. Lateral interactions and thermodynamic stability. *Metals* **8**, 311 (2018).
54. Casarin, M., Maccato, C., Vigato, N. & Vittadini, A. A theoretical study of the H_2O and H_2S chemisorption on $Cu_2O(111)$. *Appl. Surf. Sci.* **142**, 164–168 (1999).
55. Yu, X., Zhang, X., Wang, S. & Feng, G. A computational study on water adsorption on $Cu_2O(111)$ surfaces: The effects of coverage and oxygen defect. *Appl. Surf. Sci.* **343**, 33–40 (2015).
56. Chiter, F., Costa, D., Maurice, V. & Marcus, P. A DFT-based $Cu(111)||Cu_2O(111)$ model for copper metal covered by ultrathin copper oxide: structure, electronic properties and reactivity. *J. Phys. Chem. C* **124**, 17048–17057 (2020).
57. Sander, U., Strehblow, H.-H. & Dohrmann, J. K. In situ photoacoustic spectroscopy of thin oxide layers on metal electrodes. copper in alkaline solution. *J. Phys. Chem.* **85**, 447–450 (1981).
58. Finšgar, M., Peljhan, S., Kokalj, A., Kovacc, J. & Milošev, I. Determination of the Cu_2O thickness on BTAH-inhibited copper by reconstruction of Auger electron spectra. *J. Electrochem. Soc.* **157**, C295–C301 (2010).
59. Strehblow, H.-H. & Titze, B. The investigation of the passive behaviour of copper in weakly acid and alkaline solutions and the examination of the passive film by esca and ISS. *Electrochim. Acta.* **25**, 839–850 (1979).
60. Kunze, J., Maurice, V., Klein, L. H., Strehblow, H.-H. & Marcus, P. In situ scanning tunneling microscopy study of the anodic oxidation of Cu(111) in 0.1 M NaOH. *J. Phys. Chem. B* **105**, 4263–4269 (2001).
61. Kunze, J., Maurice, V., Klein, L. H., Strehblow, H.-H. & Marcus, P. In situ STM study of the duplex passive films formed on Cu(111) and Cu(001) in 0.1 M NaOH. *Corros. Sci.* **46**, 245–264 (2004).
62. Chiter, F., Costa, D., Maurice, V. & Marcus, P. DFT investigation of 2-mercaptobenzothiazole adsorption on model oxidized copper surfaces and relationship with corrosion inhibition. *Appl. Surf. Sci.* **537**, 147802 (2020).
63. Chiter, F., Costa, D., Maurice, V. & Marcus, P. Adsorption of 2-mercaptobenzimidazole corrosion inhibitor on copper: DFT study on model oxidized interfaces. *J. Electrochem. Soc.* **167**, 161506 (2020).
64. Marcus, P. & Maurice, V. Atomic level characterization in corrosion studies. *Phil. Trans. R. Soc.* **A375**, 20160414 (2016).
65. Rai, A. K., Singh, R., Singh, K. N. & Singh, V. B. FTIR, raman spectra and ab initio calculations of 2-mercaptobenzothiazole. *Spectrochim. Acta A* **63**, 483–490 (2006).
66. Mohamed, T. A. et al. Reinvestigation of benzothiazoline-2-thione and 2-mercaptobenzothiazole tautomers: Conformational stability, barriers to internal rotation and DFT calculations. *J. Mol. Struct.: THEOCHEM* **868**, 27–36 (2008).
67. Koch, H. P. Absorption spectra and structure of organic sulphur compounds. *J. Chem. Soc.* **Part III**, 401–108 (1949).
68. Chesick, J. P. & Donohue, J. The molecular and crystal structure of 2-mercaptobenzothiazole. *Acta Cryst. B* **27**, 1441–1444 (1971).
69. Geng, W. T., Nara, J. & Ohno, T. Adsorption of benzene thiolate on the (111) surface of M (M = Pt, Ag, Cu) and the conductance of m/benzene dithiolate/M molecular junctions: a first-principles study. *Thin Solid Films* **464-465**, 379–383 (2004).
70. Sun, G. et al. Performance of the vienna ab initio simulation package (VASP) in chemical applications. *J. Mol. Struct. THEOCHEM* **624**, 37–45 (2003).
71. Kresse, G. & Hafner, J. Ab initio molecular dynamics for liquid metals. *Phys. Rev. B* **47**, 558 (1993).
72. Kresse, G. & Furthmüller, J. Efficiency of ab-initio total energy calculations for metals and semiconductors using a plane-wave basis set. *Comput. Mater. Sci* **6**, 15–50 (1996).
73. Kresse, G. & Furthmüller, J. Efficient iterative schemes for ab initio total-energy calculations using a plane-wave basis set. *Phys. Rev. B* **54**, 11169–11186 (1996).
74. Kresse, G. & Joubert, D. From ultrasoft pseudopotentials to the projector augmented-wave method. *Phys. Rev. B* **59**, 1758–1775 (1999).
75. Blöchl, P. E. Projector augmented-wave method. *Phys. Rev. B* **50**, 17953 (1994).
76. Perdew, J. P. et al. Atoms, molecules, solids, and surfaces: Applications of the generalized gradient approximation for exchange and correlation. *Phys. Rev. B* **46**, 6671–6687 (1992).
77. Perdew, J. P., Burke, K. & Ernzerhof, M. Generalized gradient approximation made simple. *Phys. Rev. Lett.* **77**, 3865 (1996).
78. Methfessel, M. & Paxton, A. T. High-precision sampling for Brillouin-zone integration in metals. *Phys. Rev. B* **40**, 3616 (1989).
79. Monkhorst, H. J. & Pack, J. D. Special points for Brillonin-zone integrations. *Phys. Rev. B* **13**, 5188 (1976).
80. Dion, M., Rydberg, H., Schröder, E., Langreth, D. C. & Lundqvist, B. I. Van der Waals density functional for general geometries. *Phys. Rev. Lett.* **92**, 246401 (2004).
81. Klimeš, J., Bowler, D. R. & Michaelides, A. Chemical accuracy for the van der Waals density functional. *J. Phys.: Condens.* **22**, 022201 (2010).
82. Klimeš, J., Bowler, D. R. & Michaelides, A. Van der Waals density functionals applied to solids. *Phys. Rev. B* **83**, 195131 (2011).
83. Klimeš, J. & Michaelides, A. Perspective: Advances and challenges in treating van der Waals dispersion forces in density functional theory. *J. Chem. Phys.* **137**, 120901 (2012).
84. Kittel, C. *Introduction to Solid State Physics*, 7th edn (Wiley Sons, 1996).
85. Werner, A. & Hochheimer, H. D. High-pressure X-ray study of Cu_20 and Ag_20. *Phys. Rev. B* **25**, 5929 (1982).
86. Tang, W., Sanville, E. & Henkelman, G. A grid-based bader analysis algorithm without lattice bias. *J. Phys. Condens. Matter* **21**, 084204 (2009).

ACKNOWLEDGEMENTS

This project has received funding from the European Research Council (ERC) under the European Union's Horizon 2020 research and innovation program (ERC Advanced Grant No. 741123, Corrosion Initiation Mechanisms at the Nanometric and Atomic Scales: CIMNAS). The authors thank GENCI for high performance calculations in the national (CINES) center under the A0040802217.

AUTHOR CONTRIBUTIONS

F.C.: Methodology; Validation; Investigation; Formal analysis; Visualization; Writing—Original Draft; Writing—Review & Editing. D.C.: Resources; Supervision; Writing—Review & Editing. V. Maurice: Supervision, Writing—Review; Editing & Funding acquisition. P.M.: conceptualization, Supervision; Writing—Review and Editing; Funding acquisition & Project management.

COMPETING INTERESTS

The authors declare no competing interests.

ADDITIONAL INFORMATION

Correspondence and requests for materials should be addressed to Fatah Chiter or Philippe Marcus.

Reprints and permission information is available at http://www.nature.com/reprints

Publisher's note Springer Nature remains neutral with regard to jurisdictional claims in published maps and institutional affiliations.